Intercepting second-messenger signaling by rationally designed peptides sequestering c-di-GMP

Chee-Seng Hee[a,1], Judith Habazettl[a,1,2], Christoph Schmutz[a,1], Tilman Schirmer[a], Urs Jenal[a,2], and Stephan Grzesiek[a,2]

[a]Biozentrum, University of Basel, 4056 Basel, Switzerland

Edited by E. Peter Greenberg, University of Washington, Seattle, WA, and approved May 8, 2020 (received for review February 11, 2020)

The bacterial second messenger cyclic diguanylate (c-di-GMP) regulates a wide range of cellular functions from biofilm formation to growth and survival. Targeting a second-messenger network is challenging because the system involves a multitude of components with often overlapping functions. Here, we present a strategy to intercept c-di-GMP signaling pathways by directly targeting the second messenger. For this, we developed a c-di-GMP–sequestering peptide (CSP) that was derived from a CheY-like c-di-GMP effector protein. CSP binds c-di-GMP with submicromolar affinity. The elucidation of the CSP·c-di-GMP complex structure by NMR identified a linear c-di-GMP–binding motif, in which a self-intercalated c-di-GMP dimer is tightly bound by a network of H bonds and π-stacking interactions involving arginine and aromatic residues. Structure-based mutagenesis yielded a variant with considerably higher, low-nanomolar affinity, which subsequently was shortened to 19 residues with almost uncompromised affinity. We demonstrate that endogenously expressed CSP intercepts c-di-GMP signaling and effectively inhibits biofilm formation in *Pseudomonas aeruginosa*, the most widely used model for serious biofilm-associated medical implications.

c-di-GMP | biofilm | peptide design | protein dynamics | NMR solution structure

Bacterial second messengers are small signaling molecules that regulate a myriad of intracellular processes in response to extracellular stimuli or primary internal cues. For example, cyclic adenosine monophosphate (cAMP) controls carbon metabolism (1), (p)ppGpp has been linked to the stringent response and to nutrient stress (2), cyclic diguanylate (c-di-GMP) regulates motility, cell-cycle progression, biofilm formation, and virulence (3), cyclic GMP-AMP (3′3′-cGAMP) participates in host colonization (4) and antiphage protection (5), and cyclic adenylate (c-di-AMP) controls potassium homeostasis (6). Because second messengers act as master regulators for a wide range of important biological processes in bacteria, they are attractive drug targets to control bacterial infections. C-di-GMP signaling is widespread in gram-positive and gram-negative bacteria, including many medically important pathogens associated with multidrug resistance such as *Pseudomonas aeruginosa*, *Escherichia coli*, *Klebsiella pneumoniae*, or *Clostridium difficile* (7). Importantly, c-di-GMP is a central regulator of biofilms, multicellular bacterial communities that are engulfed in a self-produced matrix (3, 8). In the human host, pathogens often form biofilms that confer tolerance to antibiotics and host immunity, rendering classical treatment options ineffective (9). This includes chronic infections of airways of cystic fibrosis patients, urinary tract infections, and endocarditis, as well as colonization of medical implants and catheters (10). Despite the obvious medical relevance of biofilms, effective antibiofilm strategies are scarce and drugs for the specific treatment of biofilms have not been approved so far.

Interfering with c-di-GMP signaling has been proposed as a promising strategy to treat biofilm-related diseases (11, 12). C-di-GMP is synthesized and degraded by diguanylate cyclases (DGCs) and phosphodiesterases (PDEs), respectively. Increased production of c-di-GMP promotes the transition from a motile, single-cell state to a sessile lifestyle, where flagella are inactivated (13), adhesins are expressed (14), and exopolysaccharide biosynthesis is induced (15), leading to biofilm formation. In contrast, a targeted reduction of c-di-GMP prevents biofilm formation and eradicates existing biofilms (16). Consequently, specific inhibition of DGCs or activation of PDEs have been regarded as the most promising approaches to control biofilms (reviewed in refs. 17 and 18). However, bacteria often harbor multiple copies of genes encoding c-di-GMP catalysts. For instance, *P. aeruginosa* encodes 17 different proteins with a DGC domain (GGDEF), five proteins with a PDE domain (EAL or HD-GYP), and 16 proteins containing both domains (GGDE-F-EAL hybrids) (17). This diversity and redundancy of c-di-GMP turnover enzymes may represent a major challenge in the development of small molecules that globally interfere with c-di-GMP signaling pathways (18). This challenge is exacerbated by recent research showing that c-di-GMP levels are not globally regulated; some DGCs and PDEs affect local concentration, while others contribute to the overall concentration (19). Therefore, despite common catalytic mechanisms, it will be very challenging to develop highly specific and nontoxic compounds with broad effectiveness against multiple enzymes. As a universal solution to overcome this hurdle it has been proposed to directly

Significance

Cyclic diguanylate (c-di-GMP) regulates a wide range of bacterial cellular functions from biofilm formation to growth and survival. Based on the structural analysis of the complex of c-di-GMP with a bacterial effector protein followed by amino acid sequence optimization, we have developed a short peptide that binds c-di-GMP with nanomolar affinity and high specificity. This provides many opportunities for biotechnological and biomedical applications. In particular, we show that such an endogenously expressed peptide effectively reduces intracellular c-di-GMP and thereby inhibits and even disintegrates biofilms in *Pseudomonas aeruginosa*.

Author contributions: C.-S.H., J.H., C.S., T.S., U.J., and S.G. designed research; C.-S.H., J.H., and C.S. performed research; C.-S.H., J.H., and S.G. analyzed data; and C.-S.H., J.H., T.S., U.J., and S.G. wrote the paper.

The authors declare no competing interest.

This article is a PNAS Direct Submission.

Data deposition: The assignments and details of the acquired NMR spectra reported in this paper have been deposited in the Biological Magnetic Resonance Data Bank (BMRB ID codes 27990 [apo CSP1] and 50001 [CSP1·c-di-GMP]). The 10 lowest-energy structures of the CSP1·c-di-GMP complex reported in this paper have been deposited in the Protein Data Bank (PDB ID code 6SFT).

[1]C.-S.H., J.H., and C.S. contributed equally to this work.

[2]To whom correspondence may be addressed. Email: j.habazettl@unibas.ch, urs.jenal@unibas.ch, or stephan.grzesiek@unibas.ch.

This article contains supporting information online at https://www.pnas.org/lookup/suppl/doi:10.1073/pnas.2001232117/-/DCSupplemental.

First published July 1, 2020.

target the c-di-GMP molecule. Sintim and coworkers have pioneered this approach and identified several small molecules that lead to the aggregation of c-di-GMP in bacterial cells (20). Although the inhibitory effects of these small molecules are moderate, it is encouraging that c-di-GMP signaling can be manipulated by directly targeting the common product (c-di-GMP) of these enzymes.

We have recently shown that a short arginine-rich region located at the C termini of a novel family of CheY-like (Cle) proteins in *Caulobacter crescentus* binds c-di-GMP with nanomolar affinity (21). Grafting of a stretch of 36 amino acids from the C terminus of CleD onto the *E. coli* CheY protein or onto a SUMO carrier protein conveyed high c-di-GMP affinity. This indicated that the c-di-GMP binding site is fully contained within these short C-terminal peptides and prompted us to test if they could be used as c-di-GMP–sequestering peptides (CSPs). Here, we demonstrate that the C-terminal peptide from CleD is sufficient to bind c-di-GMP with nanomolar affinity, a binding affinity higher than most of the known c-di-GMP effectors (22). To reveal the structural basis for this high affinity, we determined the NMR structure and dynamics of this CSP·c-di-GMP complex. The results revealed a c-di-GMP–binding motif in which two intercalated ligand molecules are embraced by the peptide and form numerous H-bonding and cation–π interactions with arginines and stacking interactions with two tyrosine rings. An in-depth structure–activity analysis confirmed the importance of these structural motifs and allowed the development of a minimal, high-affinity CSP. Overexpression of such a CSP in *P. aeruginosa* reduced free intracellular c-di-GMP and effectively inhibited biofilm formation. These data show the potential of short peptides with high ligand-binding affinity to effectively sequester small signaling molecules like c-di-GMP. This opens the possibility to interfere with second messenger-based signaling networks in bacteria without the need to provide for specific chemical inhibitors of large families of catalysts.

Results

A Short Peptide Is Sufficient to Bind C-di-GMP with High Affinity. To obtain detailed insights into the binding mechanism of c-di-GMP to CSPs, we expressed and purified a peptide corresponding to the conserved arginine-rich C-terminal region of CleD (amino acids 140 to 174) using a standard *E. coli* system (see *Materials and Methods* for details). Isothermal calorimetry (ITC) experiments showed that this peptide, designated CSP1 (Table 1), binds c-di-GMP with a dissociation constant (K_d) of 108 nM and a stoichiometry of two c-di-GMP molecules per one CSP peptide (*SI Appendix*, Fig. S1*A*). Thus, both affinity and stoichiometry of c-di-GMP binding to CSP1 are almost identical to full-length CleD (K_d = 86 nM) (21), indicating that the short stretch of amino acids fully retains all determinants to specifically bind c-di-GMP with high affinity. This observation is remarkable since in all other known protein complexes, c-di-GMP binding involves amino acids from more than one protein region (23).

The Structure of the CSP·c-di-GMP Complex Reveals a Hitherto Unknown Binding Motif. Next, we analyzed the interaction between CSP1 and c-di-GMP by NMR. The amino acids of apo CSP1 show ^{1}H-^{15}N resonances in the central, random coil region of the HSQC (heteronuclear single quantum coherence) spectrum (Fig. 1*A*), which are indicative of an unfolded protein. In contrast, the addition of c-di-GMP to CSP1 induces large chemical shift changes toward a well-dispersed spectrum, giving evidence that the peptide has undergone a transition to a folded structure. The $^{13}C^{\alpha}$, $^{13}C^{\beta}$, and $^{13}C'$ secondary chemical shifts (Fig. 1*B*) of complexed CSP1 indicate a mixed secondary structure, with residues E143 to E146 and V151 to P153 in β-strands and residues R169 to D172 in a helical-turn conformation, respectively. Interestingly, despite its unfolded character, apo CSP1 retains about 30% propensity for the β-strands in residues E143 to E146 and V151 to P153 but no propensity for the helical turn (Fig. 1*B*).

CSP1 binding to c-di-GMP induces the appearance of four imino ^{1}H resonances in the region between 11 and 14 ppm (parts per million), which are indicative of the H-bonded imino groups in the intercalated c-di-GMP dimer (Fig. 1*D*) (24). Identical imino ^{1}H resonances were observed in the complex of c-di-GMP with full-length CleD. A comparison of the imino regions of the NOESY (nuclear Overhauser effect spectroscopy) spectra from these two complexes (Fig. 1*E*) shows identical contacts of these imino protons to the coordinating amino acids. Therefore, the CSP1 peptide binds to c-di-GMP in an identical way as to the entire CleD protein.

A well-defined three-dimensional (3D) solution structure of the CSP1·c-di-GMP complex was determined based on a total of 732 NOEs comprising 465 intrapeptide, 86 intra–c-di-GMP, and 181 intermolecular NOEs as well as 52 residual dipolar couplings, yielding a heavy-atom rmsd of 0.2 Å in the ordered region of the peptide backbone (*SI Appendix*, Table S4). The structure (Figs. 2 *C* and *D* and 3*A*) reveals that the peptide is wrapped around the self-intercalated c-di-GMP dimer with a small N-terminal β-hairpin (V145 to G152), providing a hydrophobic platform (V145, Y150) for interaction with Gua1, one of the peripheral guanine residues. Residue D154 forms a bifurcated H bond between one of its side-chain oxygens with Gua1-N1 and the main-chain amide of residue R156. This is followed by R155 and R156 that form lateral H bonds with the Hoogsteen edges of Gua1 and Gua3, respectively. Y163 stacks onto the other peripheral Gua4 and is part of a loop, which leads to R169 and D172 interacting with Gua2 and Gua4, respectively. Interestingly, the backbone of this segment is folded to a helical turn defined by the R169-O···D172-N H bond. Exactly the same arrangement occurs for the intercalated c-di-GMP bound to the RxxD motif of the functionally and structurally unrelated diguanylate cyclase PleD (Fig. 3 *A* and *B*). Apparently, this turn conformation of the main chain in CSP1 is required to properly position the side chains of R169 and D172 for H bonding with the dimeric ligand. Of note, all interacting arginines align laterally with the guanine bases, whereas in other dimeric c-di-GMP–protein complexes also head-on interactions (involving the terminal side-chain amino groups) are observed. Furthermore, the irregular conformation of the peptide allows also two main-chain groups to engage in ligand H bonding (R155-NH···Gua1-O6, K168-NH···Gua4-O6).

Besides the aforementioned H bonds, the guanidinium groups of R155, R156, and R169 form the common cation–π interactions with Gua3, Gua1, and Gua4, described in other c-di-GMP–binding proteins (25). In addition, R155 stacks with Y150 from the β-hairpin. Conspicuously, the Hoogsteen edge of Gua4 is not occupied but is in close proximity to the side chain of K168. An arginine at this position would be ideally suited to interact with the Gua4 Hoogsteen edge in a manner similar to the other three arginine–guanine pairs. Indeed, most Cle paralogs have an arginine at this position (Fig. 2*B*) and a K168R mutation of CSP1 (CSP2) increased the affinity fivefold (K_d = 19 nM; Table 1 and *SI Appendix*, Fig. S1*B*).

In summary, most of the ligand-binding functionality of CSP1 can be attributed to two conserved sequence motifs (DRR and [R/K]RxxD; Fig. 2*B*), which are separated by only 11 residues. This is distinct from other c-di-GMP–binding proteins where ligand binding invariably involves several discontinuous sequence regions separated by many amino acids. Furthermore, the CSP1 structure suggests that the c-di-GMP binding site of CleD (21) is completely defined by this relatively short domain.

Structure–Activity Relationship Defines the Minimal Requirement for C-di-GMP Binding. To obtain insights into the role of individual amino acids in the stabilization of the CSP1·c-di-GMP complex,

Table 1. CSP derivatives and their affinities to c-di-GMP

CSP	Sequence	Amino acids	K_d, nM
	140 150 160 170		
	01234567890123456789012345678901234		
1*	SKPREWVEAVAYVGPDRRRFNSADYKGPRKRKADAS	36	108
2*	SKPREWVEAVAYVGPDRRRFNSADYKGPR**R**RKADAS	36	19
3	WVEAVAYVGPDRRRFNSADYKGPR**R**RKAD	29	154
4†	DRRRFNSADYKGPR**R**RKAD	19	177
5	RRRFNSADYKGPR**R**R	15	No binding
6	RRRFNSADYKGPR**R**RKAD	18	1,406
7	DRRRFNSADYKGPR**R**RK	17	1,709
8	DRRRFNSADYKGPR**R**R	16	No binding
9	**A**RRRFNSADYKGPR**R**RKAD	19	1,754
10	D**A**RRFNSADYKGPR**R**RKAD	19	1,468
11	DR**A**RFNSADYKGPR**R**RKAD	19	1,512
12	DRR**A**FNSADYKGPR**R**RKAD	19	782
13	DRRR**A**NSADYKGPR**R**RKAD	19	140
14	DRRRF**A**SADYKGPR**R**RKAD	19	221
15	DRRRFN**A**ADYKGPR**R**RKAD	19	209
16	DRRRFNS**L**DYKGPR**R**RKAD	19	102
17	DRRRFNSA**A**YKGPR**R**RKAD	19	145
18	DRRRFNSAD**A**KGPR**R**RKAD	19	4,365
19	DRRRFNSADY**A**GPR**R**RKAD	19	261
20	DRRRFNSADYK**A**PR**R**RKAD	19	7,657
21	DRRRFNSADYKG**A**R**R**RKAD	19	346
22	DRRRFNSADYKGP**AR**RKAD	19	1,835
23	DRRRFNSADYKGPR**A**RKAD	19	4,798
24	DRRRFNSADYKGPR**RA**KAD	19	No binding
25	DRRRFNSADYKGPR**RA**AD	19	273
26	DRRRFNSADYKGPR**R**RK**L**D	19	251
27	DRRRFNSADYKGPR**R**RKA**A**	19	1,719
28	DRR-FNSADYKGPR**R**RKAD	18	1,038
29	DRRR-NSADYKGPR**R**RKAD	18	1,271
30	DRRRF-SADYKGPR**R**RKAD	18	1,253
31	DRRRFN-ADYKGPR**R**RKAD	18	439
32	DRRRFNS-DYKGPR**R**RKAD	18	338
33	DRRRFNSA-YKGPR**R**RKAD	18	437
34	DRRRFNSADYK-PR**R**RKAD	18	1,948

Sequence variations compared with CSP1 are indicated with bold letters.
*Produced using a recombinant method.
†CSP4 and CSP9 to CSP34 are acetylated at the N terminus and amidated at the C terminus.

we investigated its dynamics by ^{15}N relaxation experiments (*SI Appendix*, Fig. S2). The Lipari–Szabo order parameter S^2 (26) derived from these data is shown in Fig. 2*E*. S^2 values around 0.9 for D154, R155, R156, and R169, which are involved in H bonds to the ligand, and for A171, at the C terminus, are indicative of a well-defined structure with only small-amplitude motions of the N-H vector on the nanosecond timescale. In contrast, residues at the N and C termini, of the loop ranging from R157 to K168, and most residues of the β-hairpin have S^2 values smaller than 0.8, indicative of large nanosecond motions. Further motions in the micro- to millisecond time range are observable by chemical exchange broadening (R_{ex}) of the ^{15}N transverse relaxation rates for residues located in the N-terminal β-hairpin (Fig. 2*E*; V145, A147, A149, Y150, G152). Apparently, the β-hairpin is unstable on this timescale. The observed nano- to millisecond motions in the different regions of the CSP1·c-di-GMP complex also coincide with a low definition of the respective local structure (Fig. 2*C*).

As the β-hairpin is dynamic and only few of its residues are in van der Waals contact with the rest of the structure, we hypothesized that this part of the peptide may not be relevant for ligand binding. In order to identify the shortest CSP derivative that maintains high c-di-GMP–binding affinity, we generated several shorter CSP variants (Table 1). Since the K168R mutant peptide confers higher affinity to c-di-GMP than wild-type CSP1, this mutation was included in the peptide design of all subsequent variants. Omitting the flexible N- and C-terminal residues (variant CSP3, residues W144 to D172) reduced the affinity about eightfold (K_d = 154 nM). We then removed the entire N-terminal β-hairpin and reduced the peptide to the 19 amino acids DRRRFNSADYKGPR**R**RKAD (D154 to D172, variant CSP4). Remarkably, this drastic pruning reduced the affinity only moderately (K_d = 177 nM), in agreement with the observed dynamical instability of the N-terminal β-hairpin. Shorter variants (CSP5 to CSP8) bound the ligand very weakly or not at all (Table 1). Likewise, single amino acid deletions in the partially flexible loop from R157 to G165 resulted in significantly higher K_d values (CSP28 to CSP34; Table 1 and *SI Appendix*, Fig. S2*B*). Thus, CSP4 is the shortest CSP variant that retains high affinity to c-di-GMP.

Next, we performed single amino acid substitutions in CSP4 to characterize their role in c-di-GMP binding. All residues were replaced individually by alanine except for A161 and A171, which were replaced by leucine. The c-di-GMP affinities of these variants (CSP9 to CSP27) were measured by ITC and the results are summarized in Table 1 and Fig. 2*F*. Mutations of residues

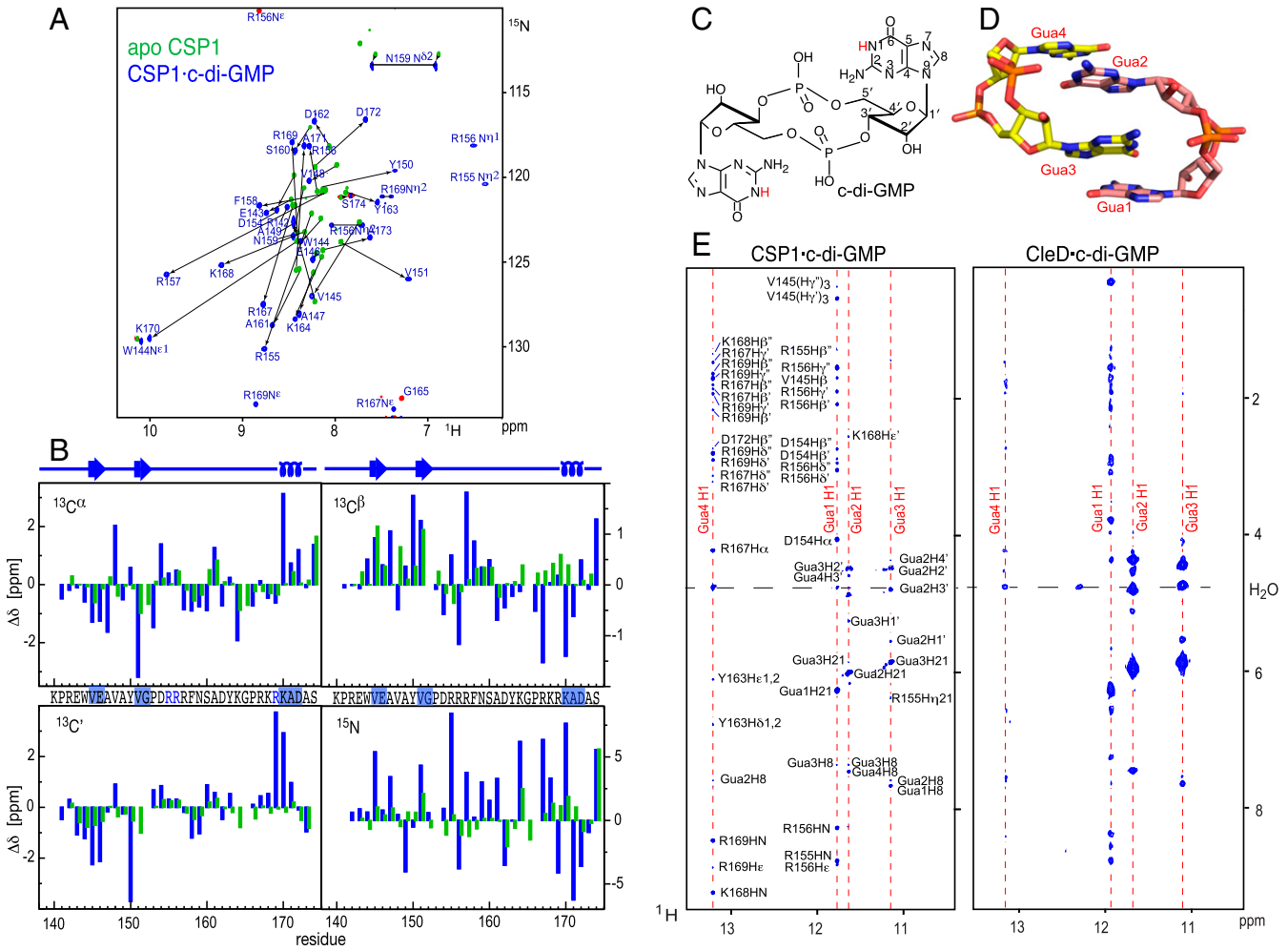

Fig. 1. Ligand binding and induced folding of CSP1. (*A*) ^{1}H-^{15}N HSQC spectra of apo CSP1 (green) and the CSP1·c-di-GMP complex (blue). Resonances are marked with assignment information. The arginine side-chain protons H^{ε}, $H^{\eta 1}$, and $H^{\eta 2}$ are in exchange with water in the apo form and are not observed. Their appearance in the complex spectrum indicates their engagement in hydrogen bonds. Resonances in red are aliased in the ^{15}N dimension and belong to the complex. (*B*) Secondary $^{13}C^{\alpha}$, $^{13}C'$, $^{13}C^{\beta}$, and ^{15}N chemical shifts of apo (green) and complex CSP1 (blue). Secondary structure elements of the CSP1·c-di-GMP complex are shown (*Top*) and highlighted in blue in the amino acid sequence of CSP1. (*C*) Chemical structure of c-di-GMP. (*D*) Structure of the intercalated c-di-GMP dimer as determined in the complex with CSP1. (*E*) Evidence for identical dimeric c-di-GMP structure and coordination in the complexes with CSP1 and full-length CleD. (*E*, *Left*) Extracted region of the 2D NOESY spectrum of the c-di-GMP·CSP1 complex showing the NOE contacts of the four imino protons H1 of guanines 1 to 4. The large numbers of c-di-GMP to peptide and c-di-GMP to c-di-GMP contacts define the ligand coordination. (*E*, *Right*) Identical region of the NOESY spectrum of the c-di-GMP·CleD complex. Identical imino proton chemical shifts and NOE contacts of the ligand dimer are observed as for the c-di-GMP·CSP1 complex.

that interact directly with c-di-GMP (D154, R155, R156, Y163, R168, R169, D172) significantly reduced the c-di-GMP–binding affinity. Strong reductions in binding also occurred for mutations of R157, G165, and R167, which are not in direct contact with the ligand in the NMR structure. G165 has a positive phi angle, disallowed for all other residue types, which is required for the backbone turn at this position (Fig. 2*D*). The side chains of R157 and R167 were not well-defined in the structure and these arginines may participate in further undetected interactions with the ligand. The replacement of all other residues that are not directly involved in c-di-GMP binding had little effect on c-di-GMP affinity. Thus, the effects of single amino acid substitutions on c-di-GMP binding agree perfectly with the NMR structural and dynamical data.

CSP Binds C-di-GMP with High Specificity. While some effector proteins that bind cyclic dinucleotide second messengers (CDNs) show high ligand specificity, others like the endoplasmic reticulum-resident protein STING can bind several CDNs (27–31). To test if CSP binds c-di-GMP specifically, we used microscale thermophoresis. Binding of c-di-GMP to CSP4 was compared with related nucleotides including GMP, GTP (guanosine triphosphate), pGpG, and four naturally occurring CDNs (3′3′-c-di-GMP, 3′3′-c-di-AMP, 3′3′-cGAMP, and 2′3′-cGAMP). As shown in *SI Appendix*, Fig. S3, only c-di-GMP binding to CSP4 was observed, while none of the related nucleotides or CDNs was able to bind to the peptide. From this, we concluded that CSP binds c-di-GMP with high affinity and specificity. This can be explained by the base-specific H-bonding interactions of Gua1 to Gua4 via their Hoogsteen edge to the guanidinium groups of the peptide arginines.

Expression of CSP Inhibits *P. aeruginosa* Biofilm Formation by Sequestering C-di-GMP. To test if CSP is able to sequester free c-di-GMP and by this inhibit biofilm formation, plasmids were constructed to express peptides from an IPTG (isopropyl β-D-1-thiogalactopyranoside)-inducible promoter (for details, see *Materials and Methods*). When CSP4 was expressed in *P. aeruginosa*, the peptide could not be detected by mass spectrometry and no

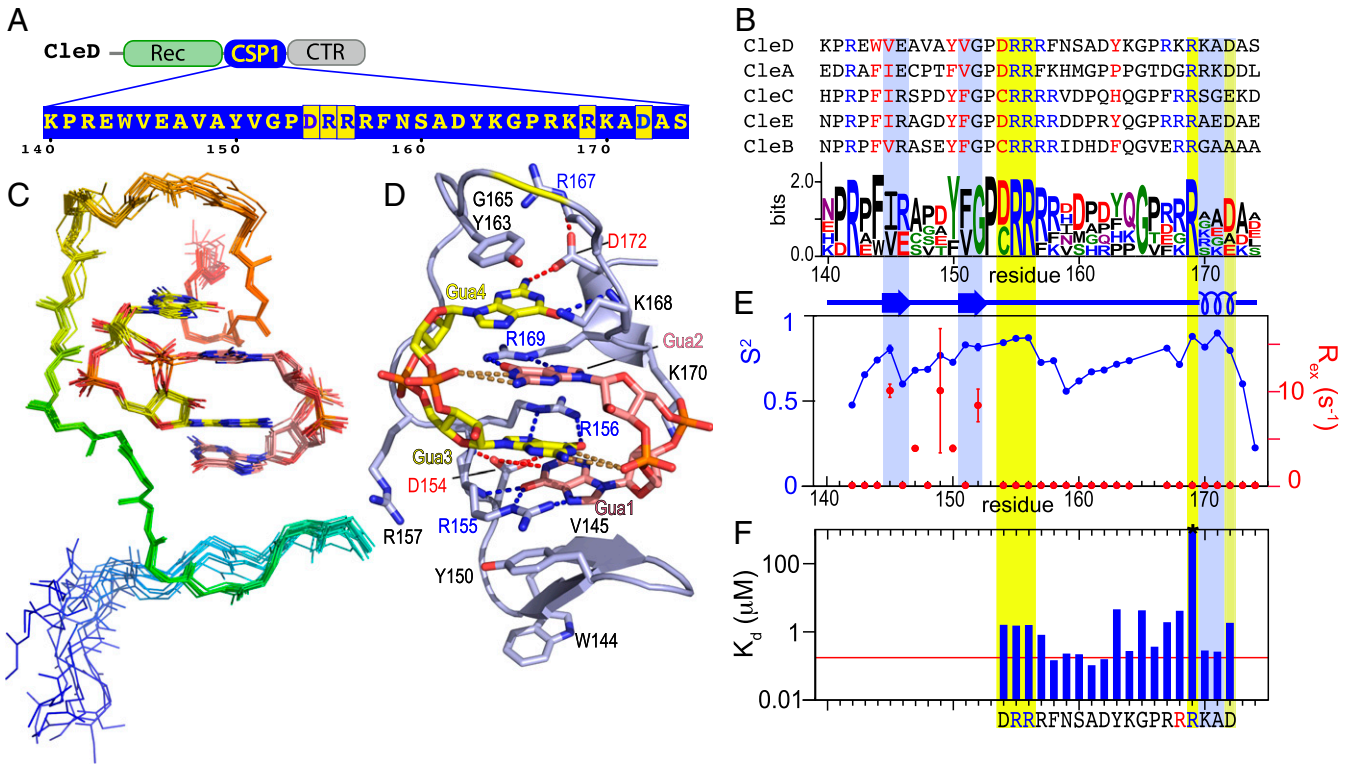

Fig. 2. Structure of CSP1·c-di-GMP, backbone dynamics, and point mutations. (*A*) CleD domain structure and CSP1 amino acid sequence. The N-terminal receiver domain (Rec) of CleD is indicated in green, the arginine-rich region CSP1 in blue, and the C-terminal region (CTR) in gray. Three arginines and two aspartic acids involved in H bonds with c-di-GMP are highlighted in yellow. (*B*) Sequence alignment of the CSP region of the CleA to D paralogs. The WebLogo3 (55) representation of this alignment (*Bottom*) emphasizes the conserved amino acids. The residue numbers stand for CleD. (*C*) Superposition of the 10 lowest-energy structures of the CSP1·c-di-GMP complex as the best fit of residues which do not exhibit large-amplitude internal motions on the nanosecond timescale: residues D154 to R157 and R167 to D172. (*D*) Lowest-energy NMR structure of intercalated dimeric c-di-GMP bound to CSP1 in ribbon representation. The orientation is similar to *C*. One c-di-GMP monomer is depicted in yellow, and the other in salmon stick representation. The side chains of W144, V145, Y150, D154, R155, R156, R157, Y163, R167, K168, R169, K170, and D172 are shown in light blue. Hydrogen bonds are depicted as dashed lines. (*E*) Backbone dynamics of holo CSP1 as derived from ^{15}N T_2, T_1, and $\{^1H\}$-^{15}N NOE relaxation data (*SI Appendix*, Fig. S2). Exchange contributions R_{ex} (red) from flexibility in the micro- to millisecond range and subnanosecond order parameters S^2 (blue) were calculated using the Lipari–Szabo model-free approach (56) with an axially symmetric diffusion model ($D_{||/\perp} = 1.95$) and overall correlation time $\tau_c = 3.8$ ns. The secondary structure is depicted (*Top*). Residues D154, R155, R156, R169, and D172 that are involved in H bonds to the ligand are highlighted in yellow. (*F*) Influence of single-point mutations on c-di-GMP binding affinity. An alanine scan (see text) of the optimized peptide CSP4 was performed and the dissociation constants were determined using ITC. The asterisk indicates no binding for CSP4-R169A. The horizontal red line shows the K_d (177 nM) of CSP4.

effect on biofilm formation was observed. Since it is well-known that short peptides are highly susceptible to proteolytic degradation (32), CSP4 was fused to Venus fluorescent protein for stability and detection. Although Venus–CSP4 expression was detected by monitoring fluorescence, the expression did not interfere with biofilm formation. We reckoned that the affinity of Venus–CSP4 might not be high enough to sequester c-di-GMP and subsequently tested CSP2, which is the variant with highest affinity. CSP2 was fused to maltose-binding protein (MBP) to improve stability and to a hexahistidine (H_6) tag for detection (Fig. 4*A*). The purified H_6-MBP–CSP2 fusion protein showed a K_d of 124.7 nM (*SI Appendix*, Fig. S1*C*), a value that is about sixfold higher than the K_d measured for CSP2 alone (*SI Appendix*, Fig. S1*B*). Thus, the hexahistidine and MBP tags seem to partially interfere with c-di-GMP binding of CSP2. Importantly, the purified H_6-MBP–CSP2-R169A control protein showed no binding of c-di-GMP (*SI Appendix*, Fig. S1*D*). In agreement with its ability to bind c-di-GMP in vitro, expression of H_6-MBP–CSP2 effectively inhibited *P. aeruginosa* biofilm formation in a concentration-dependent manner. In contrast, expression of the H_6-MBP–CSP2-R169A mutant peptide, unable to bind c-di-GMP, had no effect on biofilm formation (Fig. 4 *B* and *C*). When biofilm formation was scored over time, strains expressing the two constructs showed a similar increase during the first 8 h, before the accumulation of surface-associated biomass was blocked abruptly upon expression of the CSP2 fusion, while steadily increasing in the mutant control (Fig. 4*D*). This indicated that expression of H_6-MBP–CSP2, although unable to inhibit initial surface attachment of *P. aeruginosa* cells, was very effective in suppressing the process at later stages of biofilm formation. When peptide fusions were expressed in preformed biofilms, the c-di-GMP–specific effect, although smaller, could still be observed (Fig. 4*E*). Finally, we tested if H_6-MBP–CSP2 expression was able to reduce antibiotic-induced biofilm formation in *P. aeruginosa*. At subminimal inhibitory concentrations (MICs), antibiotics stimulate biofilm formation in *P. aeruginosa* and *E. coli*, a process that is dependent on increasing c-di-GMP concentration (33–35). As shown in *SI Appendix*, Fig. S4*A*, expression of H_6-MBP–CSP2 reduced biofilm levels both in the absence and in the presence of sub-MICs of tobramycin, but failed to "enhance" the bactericidal effects of tobramycin (*SI Appendix*, Fig. S4*B*).

Altogether, these experiments indicated that CSP expression effectively reduced biofilm formation through the specific binding and sequestration of intracellular c-di-GMP in *P. aeruginosa*. To corroborate these findings and to demonstrate that the available intracellular pool of c-di-GMP is indeed reduced, we

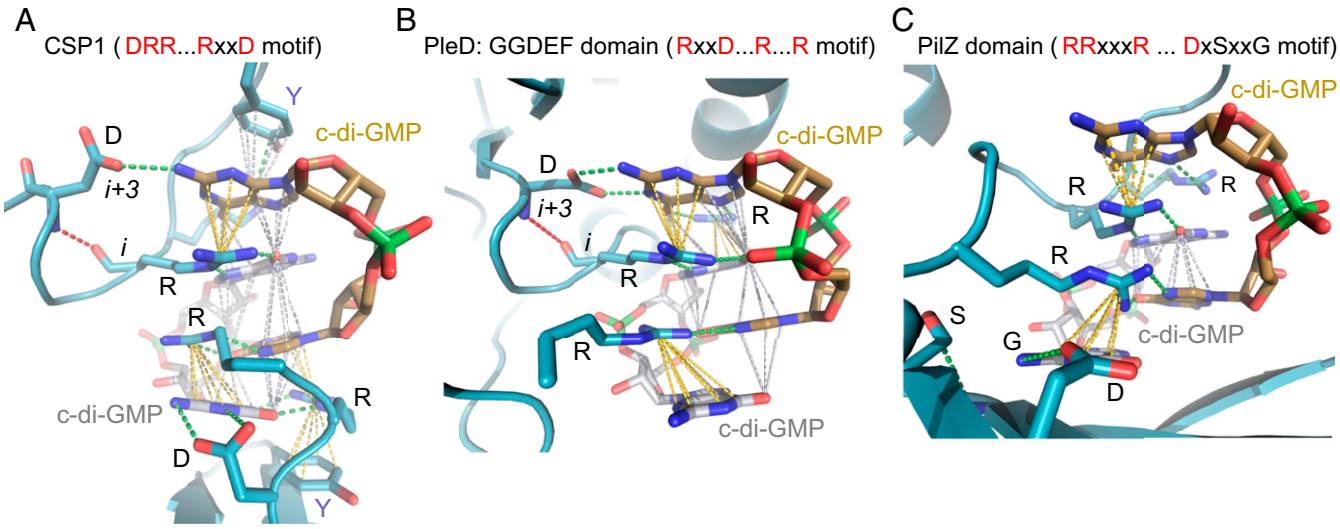

Fig. 3. Comparison of binding motifs of intercalated dimeric c-di-GMP. (*A*) The CSP1 peptide coordinates the intercalated dimeric c-di-GMP by a hitherto unknown motif. With very few exceptions (listed in *SI Appendix*, Table S5), all other known motifs for binding intercalated c-di-GMP dimers either follow the coordination found in GGDEF I site proteins or in PilZ domains. (*B* and *C*) The allosteric inhibition site of the diguanylate cyclase PleD [PDB ID code 1W25 (57)] (*B*) and the PilZ protein MapZ also known as PA4608 [PDB ID code 2L74 (24)] (*C*) are shown as representatives for these coordination motifs. An identical orientation is used for the c-di-GMP dimer with individual c-di-GMP monomers distinguished by color. H bonds are depicted as dashed green lines, cation–π interactions in yellow, and base–base stacking in gray.

made use of a fluorescence-based reporter system that specifically responds to intracellular c-di-GMP levels (36) (Fig. 5*A*). To generate the reporter, the c-di-GMP–responsive promoter of the *cdrA* gene was fused transcriptionally to the gene encoding green fluorescent protein (GFP). In the absence of c-di-GMP, the transcriptional regulator FleQ represses *cdrA* transcription. In the presence of c-di-GMP, the second messenger binds to FleQ and induces the release of FleQ from the *cdrA* promoter (37) (Fig. 5*A*). This results in a fluorescent readout of the cellular c-di-GMP levels in *P. aeruginosa*. As a positive control for the effect of decreasing c-di-GMP levels for *cdrA* promoter activity, we used sodium nitroprusside (SNP), a compound that releases nitric oxide, which in turn leads to the activation of the phosphodiesterase NbdA (38) that degrades c-di-GMP. While the expression of H_6-MBP–CSP2 effectively suppressed the synthesis of fluorescent reporter, expression of H_6-MBP–CSP2-R169A had no effect on the c-di-GMP–dependent promoter activity (Fig. 5*B*). These data strengthen the above findings that CSP interferes with the c-di-GMP signaling network in *P. aeruginosa* by directly sequestering c-di-GMP.

Discussion

Binding of c-di-GMP to proteins can be very diverse, with the nucleotide binding as a monomer, dimer, or even tetramer in different conformations (25, 39). Similar to all published structures with an intercalated dimeric c-di-GMP, the latter is stabilized in the CSP1 complex by four intermolecular H bonds between atoms H1 and H21 of the Watson–Crick edge of one molecule and the O1P atom of the other (Fig. 2*D*).

Within the five known PilZ domain structures, six GGDEF domain structures, and four other motifs which bind dimeric c-di-GMP (Fig. 3 and *SI Appendix*, Table S5), H bond and cation–π interactions with the ligand are formed by arginines and aspartates distributed over several separate ligand-binding regions. In contrast, in CSP1, the ligand binding is confined to a short consecutive stretch of amino acids where three arginines interact laterally with the Hoogsteen edges of Gua1, Gua2, and Gua3, while D154 and D172 form H bonds with Gua1 and Gua4, respectively. Thus, CSP1 binds c-di-GMP specifically and with high affinity via a DRR-x_{11}-(R/K)RxxD motif. Notably, apo CSP1 is largely unstructured, with a 30% β-sheet propensity for the residues that form the β-hairpin in the complexed structure. Upon binding of c-di-GMP, apo CSP1 undergoes a classical binding and folding transition (40). Further dynamic and structure–activity studies identified a 19-amino acid-long peptide with improved affinity. Currently, no other highly specific, small-molecular mass binder to c-di-GMP exists and this peptide sequence may have technical applications such as sensor development and affinity chromatography.

Based on these findings, we have developed an approach to inhibit biofilms by directly sequestering c-di-GMP using a peptide with high binding affinity in a proof-of-principle study. The approach overcomes the redundancy of c-di-GMP turnover enzymes by directly targeting the common product (c-di-GMP) of these enzymes, resulting in a more effective and universal control of bacterial biofilms. An effective method for the disintegration of biofilms would be an important step in the development of new antibacterial strategies and to address the worldwide threat of antibiotic resistance.

Our study provides the foundation for the development of a peptide-based antibiofilm agent. However, we anticipate several major challenges ahead with regard to the diffusion of the peptide through existing biofilms, its uptake by bacterial cells, and its stability outside and inside bacterial cells. Several strategies have been reported that may overcome these hurdles. For example, peptides can be combined with biofilm-"disrupting" molecules such as EDTA (ethylenediaminetetraacetate) or DNase, which have been shown to largely enhance the efficacies of antimicrobials (41, 42). To facilitate bacterial uptake, peptides can be fused to cell-penetrating peptides (43). Finally, chemical modifications can prevent proteolytic degradation and improve the in vivo half-life of peptide drugs (44).

The peptide-sequestering approach may not be limited to targeting the intercalated c-di-GMP dimer. A number of structures exist in the Protein Data Bank of protein complexes with other CDNs such as c-di-AMP and the mixed-linkage cGMP-AMP (2′3′-cGAMP). The latter plays a central role in human and mouse cGAS/STING pathways, which are involved in the immune response to viral infection and tumorigenesis as well as in autoimmune diseases (45). High-affinity peptides that, for

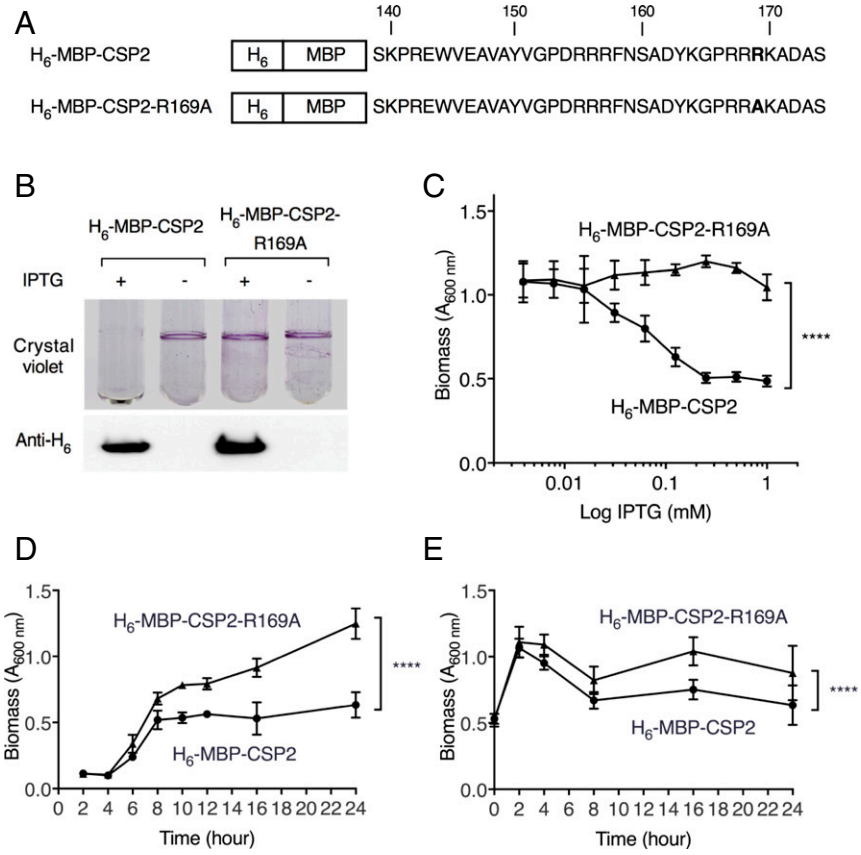

Fig. 4. Expression of CSP fusion protein inhibits *P. aeruginosa* biofilm formation. (*A*) H_6-MBP–CSP2 and H_6-MBP–CSP2-R169A fusion constructs used in this study. CSP amino acid sequences are represented in one-letter code with residue numbers according to the numbering of CleD. Bold letters highlight the R169A mutation that prevents c-di-GMP binding. (*B*) Expression of H_6-MBP–CSP2 inhibits biofilm formation on glass tubes while expression of the mutant construct has no effect. The biofilm rings formed at the liquid–air interfaces were stained with crystal violet. (*B*, *Bottom*) Protein expression levels were verified by Western blot using an anti-hexahistidine antibody. (*C*) H_6-MBP–CSP2 expression-dependent biofilm reduction is tunable. IPTG titration leads to a dose-dependent biofilm reduction through H_6-MBP–CSP2 expression whereas no obvious effect of the mutant construct is observed. The biomass upon H_6-MBP–CSP2 expression is significantly less than that of the mutant at a concentration of 1 mM IPTG; $^{****}P < 0.0001$ (*t* test). Error bars represent the SD of four different experiments. (*D*) Biofilm formation upon induction of expression with 1 mM IPTG over the course of 24 h. The biomass of H_6-MBP–CSP2 is significantly less than that of the mutant after 24 h of induction; $^{****}P < 0.0001$ (*t* test). Data are shown as means ± SD ($n = 2$). (*E*) Eradication of preformed biofilms upon H_6-MBP–CSP2 expression. Biofilms were allowed to grow for 8 h before induction with 1 mM IPTG for 16 h. The biomass of H_6-MBP–CSP2 is significantly less than that of the mutant after 16 h of induction; $^{****}P < 0.0001$ (*t* test). Data are shown as means ± SD ($n = 2$).

example, target 2′3′-cGAMP could reduce inflammation in autoimmune diseases. While specific recognition of 2′3′-cGAMP and other CDNs in the complex structures solved so far occurs similarly to most c-di-GMP complexes via discontinuous ligand-binding regions, their combination into shorter peptides may be possible by peptide engineering or directed evolution methods.

In summary, the development of a short peptide that binds c-di-GMP with high affinity and specificity provides opportunities for biotechnological and biomedical applications. The specific c-di-GMP sequestration presents an alternative strategy to current drug discovery and development practices by targeting a signaling molecule that plays a key role in the formation of biofilms and bacterial persistence. Although many obstacles are anticipated and remain to be solved before such an active compound can be developed, the ability to "directly" interfere with a central signaling pathway makes this a promising approach that deserves further exploration.

Materials and Methods

Strains, Plasmids, and Growth Conditions. The bacterial strains, plasmids, and oligonucleotides used in this study are listed in *SI Appendix*, Tables S1–S3, respectively. *P. aeruginosa* and *E. coli* were grown in lysogeny broth (LB) at 37 °C containing the appropriate selective antibiotic when required.

To construct the plasmid pET28a-H6-SUMO-CSP2 for CSP2 peptide production, the mutagenesis to introduce K168R was performed on the plasmid pET28a-H6-SUMO-CSP1 (for this plasmid construction, see ref. 21) using primers prCSH1 and prCSH2. The plasmid pME6032-H6-SUMO-CSP2 (pTP16) was constructed by inserting the *Nco*I- and *Xho*I-restricted DNA fragment of H6-SUMO-CSP2 from pET28a-H6-SUMO-CSP2 into the same restriction sites of the pME6032 plasmid. A restriction-free cloning method (46) was used to generate the plasmid pME6032-CSP4 (pTP1). Primers prTP1 and prTP2 were used to prepare CSP4 megaprimers, which were then used to introduce the CSP4 sequence into the pME6032 plasmid. The plasmid pME6032-CSP2 (pTP33) was constructed by inserting the amplified DNA fragment of CSP2 into the *Eco*RI and *Sac*I restriction sites of pME6032. Primers prTP56 and prTP57 were used to generate the CSP2 fragment.

The plasmid pME6032-H6-MBP-CSP2-0 (pTP18) was constructed using a restriction-free cloning method. First, megaprimers containing the MBP sequence were prepared from the plasmid pETG41A-H6-MBP with the primers prTP28 and prTP29. In the secondary PCR, the megaprimers were used to replace SUMO with MBP in the plasmid pME6032-H6-SUMO-CSP2 that yielded the plasmid pME6032-H6-MBP-CSP2. The same procedure was carried out to generate pME6032-H6-TRX-CSP2-0 (pTP19) and pME6032-H6-DsbA-CSP2-0 (pTP20) by using the primer pairs prTP31–prTP32 and prTP35–prTP36 and the plasmids pETG20A-TRX-H6 and pETG52A-llDsbA-H6, respectively. The three constructs had low levels of expression and, to enhance the expression, the distance of the ribosomal binding site to the start codon ATG of the three constructs was optimized. The primer pair prTP49–prTP50 was used to produce pME6032-H6-MBP-CSP2 (pTP23) and prTP50–prTP51 for both pME6032-H6-TRX-CSP2

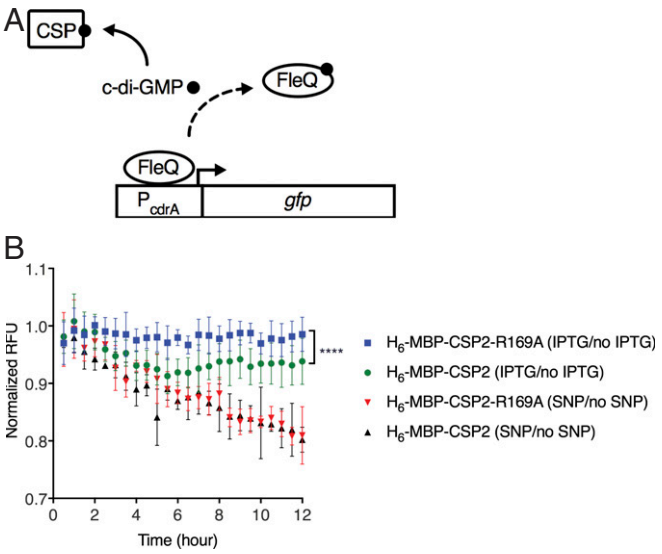

Fig. 5. Expression of H_6-MBP–CSP2 suppressed fluorescent signal increment in a c-di-GMP reporter system. (*A*) Schematic concept showing that CSP sequesters c-di-GMP away from the repressor FleQ in the reporter system, resulting in suppression of GFP fluorescent signals. (*B*) The fluorescent signals are shown as a ratio between treatment (IPTG or SNP) and no treatment. An unchanged ratio as shown for H_6-MBP–CSP2-R169A (IPTG/no IPTG) indicates that IPTG induction did not suppress the increment of fluorescent signal. On the other hand, IPTG-induced H_6-MBP–CSP2 significantly suppressed the fluorescence, indicating that the CSP2 fusions effectively sequestered c-di-GMP away from the transcription regulator FleQ. SNP treatment in both strains suppressed fluorescence increment. RFU, relative fluorescence unit. The difference between H_6-MBP–CSP2 and H_6-MBP–CSP2-R169A signals at 12 h is statistically significant; $^{****}P < 0.0001$ (*t* test). Data are shown as means ± SD ($n = 3$).

(pTP22) and pME6032-H6-DsbA-CSP2 (pTP24). The R169A mutation was introduced by site-directed mutagenesis using the primers prTP54 and prTP55 that carry the R169A mutation. This resulted in three plasmids that contain the mutations: pME6032-H6-DsbA-CSP2-R169A (pTP24), pME6032-H6-MBP-CSP2-R169A (pTP31), and pME6032-H6-TRX-CSP2-R169A (pTP32).

All constructs were transformed into *E. coli* DH5α for storage and plasmid preparation. All constructs were verified by DNA sequencing before transformation into *E. coli* Rosetta for peptide production or *P. aeruginosa* PAO1 (UJP505).

Protein and Peptide Expression and Purification. The peptides CSP1 and CSP2 as well as H_6-CleD were produced using the following protocol. Briefly, the plasmids (see *SI Appendix*, Table S2 for details) were transformed into Rosetta (DE3) cells. Protein expression was induced with 0.5 mM IPTG at an OD_{600} of 0.5 for 4 h at 37 °C. Cells from a 2-L culture were collected by centrifugation at 4,500 × *g* for 15 min and then frozen at −20 °C. Pellets were thawed and dissolved in 10 mL binding buffer (50 mM Tris·HCl, pH 8, 500 mM NaCl, 5 mM $MgCl_2$, 30 mM imidazole), followed by sonication at 40% output power for 3 min with a repeated interval of a 1-s pulse and a 2-s pause. Lysed cells were centrifuged at 164,700 × *g* for 30 min. The cell lysate was loaded onto a 1-mL HisTrap column (GE Healthcare). The column was then washed and the bound samples were eluted with elution buffer (50 mM Tris·HCl, pH 8, 500 mM NaCl, 5 mM $MgCl_2$, 500 mM imidazole) in an eight-column volume gradient. Elution fractions were assessed by SDS-PAGE (sodium dodecyl sulfate-polyacrylamide gel electrophoresis) to detect expressed protein fractions. Fractions containing expressed proteins were pooled and concentrated using a protein concentrator with a molecular mass cutoff of 10 kDa (Millipore). Samples were loaded onto a Superdex S75 10/30 column (GE Healthcare) preequilibrated with gel-filtration buffer (50 mM Tris·HCl, pH 8, 100 mM NaCl, 5 mM $MgCl_2$) and the protein fractions were assessed by SDS-PAGE.

To remove the peptides CSP1 and CSP2 from H_6-SUMO, SUMO protease ULP1 was added to purified H_6-SUMO-CSP1 and H_6-SUMO-CSP2 at a ratio of 5 μg to 1 mg fusion protein. The mixture was incubated at 25 °C for 16 h. The digested sample was loaded onto a preequilibrated 1-mL HisTrap column to remove H_6-SUMO. The flowthrough containing the peptides was collected and assessed by SDS-PAGE. Fractions containing CSP peptides were pooled, concentrated to 1 mL, and loaded onto a Superdex S75 10/30 column preequilibrated with gel-filtration buffer. Eluted fractions were assessed by SDS-PAGE.

To prepare the isotope-labeled samples for NMR analyses, the pET28a-H6-SUMO-CSP1 construct was transformed into Rosetta (DE3) cells and expressed by growing the cells in 3 L of minimal medium containing 1.5 g of $^{15}NH_4Cl$ and 4.8 g of unlabeled or ^{13}C-labeled glucose as sole nitrogen and carbon sources, respectively. Peptide cleavage and purification protocols were as described above.

Peptide Synthesis. Lyophilized peptides with at least 95% purity, except for FITC (fluorescein isothiocyanate)-labeled peptides with at least 70% purity, were purchased from ProteoGenix or GenScript. Peptides were dissolved in ultrapure water and the concentrations were determined using a NanoDrop spectrophotometer (Thermo Scientific).

NMR Spectroscopy, Resonance Assignments, and Structure Calculations. Uniformly ^{13}C-^{15}N– and ^{15}N-labeled samples of CSP1 (0.9 to 1.0 mM) were prepared in 100 mM NaCl, 20 mM phosphate, 2 mM $MgCl_2$, 0.01% NaN_3 (wt/vol; weight/volume), 5% (vol/vol) D_2O (pH 6.5) as sample volumes of 270 μL. For complex formation, 10 mM c-di-GMP (BioLog) was titrated to the apo CSP1 sample and the fraction of apo and ligand-bound protein was monitored by ^1H-^{15}N HSQC spectra. The titration was stopped at a molar ratio of 3:1 (c-di-GMP:CSP1), at which binding had reached saturation. Nonisotropic samples of complexed protein were prepared by adding 17 mg/mL filamentous phage Pf1 (Asia Biotech). Unlabeled full-length CleD samples (500 μM) with (molar ratio 3:1) or without c-di-GMP were prepared in 200 mM NaCl, 20 mM phosphate, 1 mM $MgCl_2$, 0.01% NaN_3 (wt/vol), 5% (vol/vol) D_2O (pH 7.0) as sample volumes of 270 μL.

All NMR spectra were recorded at 298 K on Bruker DRX 600 and DRX 900 NMR spectrometers equipped with TXI and TCI probe heads, respectively. For resonance assignment and structure and dynamical information, standard 2D and 3D NMR assignment, NOE, residual dipolar coupling, and relaxation experiments were acquired similar to the ones described (47). NMR data were processed using the NMRPipe suite of programs (48). Spectra were displayed and analyzed with the programs SPARKY (49) and PIPP (50). Structure calculations were performed with the program Xplor-NIH (51) using a simulated annealing protocol (52) with the c-di-GMP molecules defined as two-residue, circular strands of RNA. A total of 200 structures were calculated and the 10 lowest-energy structures were selected for deposition in the Protein Data Bank (PDB ID code 6SFT). The structural statistics are given in *SI Appendix*, Table S4.

Biofilm Assay. The protocol of a standard biofilm assay was followed with minor modifications (53). Briefly, *P. aeruginosa* biofilms were grown at 37 °C without agitation in LB in 96-well plates (Falcon; 353072). After 24 h, the optical density (OD) was measured at 600 nm in a microtiter plate reader (EL800; BioTek) to determine bacterial growth. The plates were subsequently rinsed three times with demineralized water to remove nonattached bacteria. The adherent biofilms were stained with 0.1% crystal violet and dissolved in 20% acetic acid, allowing quantification by measuring the OD_{600} in the microtiter plate reader.

Isothermal Titration Calorimetry. ITC experiments were performed on a VP-ITC or ITC200 microcalorimeter (MicroCal). Proteins, peptide, c-di-GMP, and buffer (50 mM Tris·HCl, pH 8.0, 100 mM NaCl) were degassed for 15 min prior to filling into the sample cell and syringe. All measurements were performed at 15 °C. For measurements performed on a VP-ITC, the sample cell contained about 10 μM protein or peptide and the syringe contained about 200 μM c-di-GMP, with 30 injections (10 μL each) and a 250-s interval. For ITC200, the sample cell contained about 20 μM c-di-GMP and the syringe contained about 100 μM protein or peptide, with 18 injections (2 μL each) and a 120-s interval. The concentrations were determined on a spectrophotometer using a cuvette with a 1-cm path length. The data were analyzed using ITC Data Analysis in ORIGIN (MicroCal) provided by the manufacturer.

Microscale Thermophoresis. The binding of c-di-GMP and related nucleotides to N-terminally FITC-labeled CSP4 (FITC-CSP4-NH_2) was determined on a Monolith NT.115 instrument with standard-treated capillaries (NanoTemper Technologies). Fluorescence changes were recorded using blue channel optics of the instrument for a 30-s period of infrared laser heating at 50% of maximum laser power followed by a cooling period of 5 s. The measurement

buffer consisted of 50 mM Tris·HCl (pH 8.0), 100 mM NaCl, and 0.1% polysorbate 20.

Fluorescent C-di-GMP Reporter. A fluorescent c-di-GMP reporter system was used as previously described (36) and modified (54). The reporter consisted of the c-di-GMP–responsive *cdrA* promoter transcriptionally fused to genes encoding GFP. *P. aeruginosa* PAO1 strains containing the CSP expression vectors (pTP23 and pTP31) were transformed with the pCdrA::*gfp* pUCP22-*Not*I–based c-di-GMP–level reporter plasmid (54). The bacteria containing both plasmids were grown overnight in LB containing the appropriate antibiotics. The overnight cultures were diluted 1:50 in LB and grown at 37 °C on a shaker (170 rpm) until an OD_{600} of 0.3 was reached. Bacteria were transferred to 96-well clear-bottom black-side plates (Costar) where IPTG or SNP (Sigma) was added. Fluorescence (GFP: 485 nm/515 nm) and OD_{600} were recorded every 30 min for 24 h using a Synergy H4 plate reader (BioTek).

SDS-PAGE and Immunoblotting. Bacteria were grown in LB in the presence of 1 mM IPTG to induce expression of the proteins. Afterward, the cells were diluted to an OD_{600} of 1. Cells were lysed by addition of SDS sample buffer and boiled for 5 min at 99 °C. The samples were subjected to SDS-polyacrylamide gels (Bio-Rad) and electroblotted onto nitrocellulose membranes with a Trans-Blot SD Semi-Dry Transfer Cell (Bio-Rad). Membranes were blocked for 1 h with 5% milk, 0.1% Tween 20 PBS (phosphate-buffered saline) at room temperature followed by primary antibody application at 4 °C with a mouse anti-His antibody (GE Healthcare) diluted in 5% milk, 0.1% Tween 20 PBS. Horseradish peroxidase-conjugated secondary antibodies were purchased from Cell Signaling Technology. The blots were developed with an enhanced chemiluminescence reagent (LumiGlo Reserve; KPL) and imaged using an ImageQuant LAS-4000 System (Fujitsu Life Sciences).

Data Availability. The assignments and details of the acquired NMR spectra have been deposited in the Biological Magnetic Resonance Data Bank (BMRB ID codes 27990 [apo CSP1] and 50001 [CSP1·c-di-GMP]). The 10 lowest-energy structures of the CSP1·c-di-GMP complex have been deposited in the Protein Data Bank (PDB ID code 6SFT).

ACKNOWLEDGMENTS. We gratefully acknowledge Dr. Timothy Sharpe of the Biozentrum Biophysics Facility for expert help with the biophysical characterization of CSP. This work was supported by the Swiss Commission for Technology and Innovation (Grant 18366.1 PFLS-LS to C.-S.H., C.S., U.J., and T.S.) and Swiss National Science Foundation (Grants 31-149927 and 31-173089 to S.G., Grant 31-166652 to T.S., and Grant 31-147090 to U.J.).

1. K. A. McDonough, A. Rodriguez, The myriad roles of cyclic AMP in microbial pathogens: From signal to sword. *Nat. Rev. Microbiol.* **10**, 27–38 (2011).
2. Z. D. Dalebroux, M. S. Swanson, ppGpp: Magic beyond RNA polymerase. *Nat. Rev. Microbiol.* **10**, 203–212 (2012).
3. U. Jenal, A. Reinders, C. Lori, Cyclic di-GMP: Second messenger extraordinaire. *Nat. Rev. Microbiol.* **15**, 271–284 (2017).
4. B. W. Davies, R. W. Bogard, T. S. Young, J. J. Mekalanos, Coordinated regulation of accessory genetic elements produces cyclic di-nucleotides for *V. cholerae* virulence. *Cell* **149**, 358–370 (2012).
5. D. Cohen *et al*., Cyclic GMP-AMP signalling protects bacteria against viral infection. *Nature* **574**, 691–695 (2019).
6. J. Gundlach *et al*., Control of potassium homeostasis is an essential function of the second messenger cyclic di-AMP in *Bacillus subtilis*. *Sci. Signal.* **10**, eaal3011 (2017).
7. C. L. Hall, V. T. Lee, Cyclic-di-GMP regulation of virulence in bacterial pathogens. *Wiley Interdiscip. Rev. RNA* **9**, e1454 (2018).
8. U. Römling, M. Y. Galperin, M. Gomelsky, Cyclic di-GMP: The first 25 years of a universal bacterial second messenger. *Microbiol. Mol. Biol. Rev.* **77**, 1–52 (2013).
9. U. Römling, C. Balsalobre, Biofilm infections, their resilience to therapy and innovative treatment strategies. *J. Intern. Med.* **272**, 541–561 (2012).
10. P. Gupta, S. Sarkar, B. Das, S. Bhattacharjee, P. Tribedi, Biofilm, pathogenesis and prevention—A journey to break the wall: A review. *Arch. Microbiol.* **198**, 1–15 (2016).
11. T. Bjarnsholt, O. Ciofu, S. Molin, M. Givskov, N. Høiby, Applying insights from biofilm biology to drug development—Can a new approach be developed? *Nat. Rev. Drug Discov.* **12**, 791–808 (2013).
12. S. Wagner *et al*., Novel strategies for the treatment of *Pseudomonas aeruginosa* infections. *J. Med. Chem.* **59**, 5929–5969 (2016).
13. A. Boehm *et al*., Second messenger-mediated adjustment of bacterial swimming velocity. *Cell* **141**, 107–116 (2010).
14. K. S. Sprecher *et al*., Cohesive properties of the *Caulobacter crescentus* holdfast adhesin are regulated by a novel c-di-GMP effector protein. *MBio* **8**, e00294-17 (2017).
15. D. Pérez-Mendoza, J. Sanjuán, Exploiting the commons: Cyclic diguanylate regulation of bacterial exopolysaccharide production. *Curr. Opin. Microbiol.* **30**, 36–43 (2016).
16. L. D. Christensen *et al*., Clearance of *Pseudomonas aeruginosa* foreign-body biofilm infections through reduction of the cyclic di-GMP level in the bacteria. *Infect. Immun.* **81**, 2705–2713 (2013).
17. H. Kulasakara *et al*., Analysis of *Pseudomonas aeruginosa* diguanylate cyclases and phosphodiesterases reveals a role for bis-(3′-5′)-cyclic-GMP in virulence. *Proc. Natl. Acad. Sci. U.S.A.* **103**, 2839–2844 (2006).
18. C. Opoku-Temeng, J. Zhou, Y. Zheng, J. Su, H. O. Sintim, Cyclic dinucleotide (c-di-GMP, c-di-AMP, and cGAMP) signalings have come of age to be inhibited by small molecules. *Chem. Commun. (Camb.)* **52**, 9327–9342 (2016).
19. R. Hengge, Principles of c-di-GMP signalling in bacteria. *Nat. Rev. Microbiol.* **7**, 263–273 (2009).
20. S. Nakayama, J. Zhou, Y. Zheng, H. Szmacinski, H. O. Sintim, Supramolecular polymer formation by cyclic dinucleotides and intercalators affects dinucleotide enzymatic processing. *Future Sci. OA* **2**, FSO93 (2016).
21. J. Nesper *et al*., Cyclic di-GMP differentially tunes a bacterial flagellar motor through a novel class of CheY-like regulators. *eLife* **6**, e28842 (2017).
22. I. S. Pultz *et al*., The response threshold of *Salmonella* PilZ domain proteins is determined by their binding affinities for c-di-GMP. *Mol. Microbiol.* **86**, 1424–1440 (2012).
23. T. Schirmer, C-di-GMP synthesis: Structural aspects of evolution, catalysis and regulation. *J. Mol. Biol.* **428**, 3683–3701 (2016).
24. J. Habazettl, M. G. Allan, U. Jenal, S. Grzesiek, Solution structure of the PilZ domain protein PA4608 complex with cyclic di-GMP identifies charge clustering as molecular readout. *J. Biol. Chem.* **286**, 14304–14314 (2011).
25. S.-H. Chou, M. Y. Galperin, Diversity of cyclic di-GMP-binding proteins and mechanisms. *J. Bacteriol.* **198**, 32–46 (2016).
26. G. Lipari, A. Szabo, Model-free approach to the interpretation of nuclear magnetic resonance relaxation in macromolecules. *J. Am. Chem. Soc.* **104**, 4546–4559 (1983).
27. D. L. Burdette *et al*., STING is a direct innate immune sensor of cyclic di-GMP. *Nature* **478**, 515–518 (2011).
28. O. Danilchanka, J. J. Mekalanos, Cyclic dinucleotides and the innate immune response. *Cell* **154**, 962–970 (2013).
29. S. Ouyang *et al*., Structural analysis of the STING adaptor protein reveals a hydrophobic dimer interface and mode of cyclic di-GMP binding. *Immunity* **36**, 1073–1086 (2012).
30. N. Shaw, S. Ouyang, Z.-J. Liu, Binding of bacterial secondary messenger molecule c di-GMP is a STING operation. *Protein Cell* **4**, 117–129 (2013).
31. X. Zhang *et al*., Cyclic GMP-AMP containing mixed phosphodiester linkages is an endogenous high-affinity ligand for STING. *Mol. Cell* **51**, 226–235 (2013).
32. Y. Li, Recombinant production of antimicrobial peptides in *Escherichia coli*: A review. *Protein Expr. Purif.* **80**, 260–267 (2011).
33. J. B. Kaplan, Antibiotic-induced biofilm formation. *Int. J. Artif. Organs* **34**, 737–751 (2011).
34. L. R. Hoffman *et al*., Aminoglycoside antibiotics induce bacterial biofilm formation. *Nature* **436**, 1171–1175 (2005).
35. A. Boehm *et al*., Second messenger signalling governs *Escherichia coli* biofilm induction upon ribosomal stress. *Mol. Microbiol.* **72**, 1500–1516 (2009).
36. M. T. Rybtke *et al*., Fluorescence-based reporter for gauging cyclic di-GMP levels in *Pseudomonas aeruginosa*. *Appl. Environ. Microbiol.* **78**, 5060–5069 (2012).
37. J. W. Hickman, C. S. Harwood, Identification of FleQ from *Pseudomonas aeruginosa* as a c-di-GMP-responsive transcription factor. *Mol. Microbiol.* **69**, 376–389 (2008).
38. Y. Li, S. Heine, M. Entian, K. Sauer, N. Frankenberg-Dinkel, NO-induced biofilm dispersion in *Pseudomonas aeruginosa* is mediated by an MHYT domain-coupled phosphodiesterase. *J. Bacteriol.* **195**, 3531–3542 (2013).
39. T. Schirmer, U. Jenal, Structural and mechanistic determinants of c-di-GMP signalling. *Nat. Rev. Microbiol.* **7**, 724–735 (2009).
40. K. Sugase, H. J. Dyson, P. E. Wright, Mechanism of coupled folding and binding of an intrinsically disordered protein. *Nature* **447**, 1021–1025 (2007).
41. Z. Liu *et al*., In vitro and in vivo activity of EDTA and antibacterial agents against the biofilm of mucoid *Pseudomonas aeruginosa*. *Infection* **45**, 23–31 (2017).
42. R. Cavaliere, J. L. Ball, L. Turnbull, C. B. Whitchurch, The biofilm matrix destabilizers, EDTA and DNaseI, enhance the susceptibility of nontypeable *Hemophilus influenzae* biofilms to treatment with ampicillin and ciprofloxacin. *MicrobiologyOpen* **3**, 557–567 (2014).
43. K. A. Brogden, Antimicrobial peptides: Pore formers or metabolic inhibitors in bacteria? *Nat. Rev. Microbiol.* **3**, 238–250 (2005).
44. K. Fosgerau, T. Hoffmann, Peptide therapeutics: Current status and future directions. *Drug Discov. Today* **20**, 122–128 (2015).
45. J. Tao, X. Zhou, Z. Jiang, cGAS-cGAMP-STING: The three musketeers of cytosolic DNA sensing and signaling. *IUBMB Life* **68**, 858–870 (2016).
46. S. R. Bond, C. C. Naus, RF-cloning.org: An online tool for the design of restriction-free cloning projects. *Nucleic Acids Res.* **40**, W209–W213 (2012).
47. S. Grzesiek *et al*., Refined solution structure and backbone dynamics of HIV-1 Nef. *Protein Sci.* **6**, 1248–1263 (1997).

48. F. Delaglio *et al*., NMRPipe: A multidimensional spectral processing system based on UNIX pipes. *J. Biomol. NMR* **6**, 277–293 (1995).
49. T. D. Goddard, D. G. Kneller, SPARKY 3 (University of California, San Francisco, CA, 2008).
50. D. Garrett, R. Powers, A. Gronenborn, G. Clore, A common sense approach to peak picking in two-, three-, and four dimensional spectra using automatic computer analysis of contour diagrams. *J. Magn. Reson.* **95**, 214–220 (1991).
51. C. D. Schwieters, J. J. Kuszewski, N. Tjandra, G. M. Clore, The Xplor-NIH NMR molecular structure determination package. *J. Magn. Reson.* **160**, 65–73 (2003).
52. M. Nilges, G. M. Clore, A. M. Gronenborn, Determination of three-dimensional structures of proteins from interproton distance data by hybrid distance geometry-dynamical simulated annealing calculations. *FEBS Lett.* **229**, 317–324 (1988).
53. G. A. O'Toole *et al*., Genetic approaches to study of biofilms. *Methods Enzymol.* **310**, 91–109 (1999).
54. U. N. Broder, T. Jaeger, U. Jenal, LadS is a calcium-responsive kinase that induces acute-to-chronic virulence switch in *Pseudomonas aeruginosa*. *Nat. Microbiol.* **2**, 16184 (2016).
55. G. E. Crooks, G. Hon, J. M. Chandonia, S. E. Brenner, WebLogo: A sequence logo generator. *Genome Res.* **14**, 1188–1190 (2004).
56. G. Lipari, A. Szabo, Model-free approach to the interpretation of nuclear magnetic resonance relaxation in macromolecules. 2. Analysis of experimental results. *J. Am. Chem. Soc.* **104**, 4559–4570 (1982).
57. C. Chan *et al*., Structural basis of activity and allosteric control of diguanylate cyclase. *Proc. Natl. Acad. Sci. U.S.A.* **101**, 17084–17089 (2004).